Prostate-specific membrane antigen cleavage of vitamin B9 stimulates oncogenic signaling through metabotropic glutamate receptors

Charalambos Kaittanis,[1,5] Chrysafis Andreou,[2] Haley Hieronymus,[3] Ninghui Mao,[3] Catherine A. Foss,[6] Matthias Eiber,[7] Gregor Weirich,[8] Palak Panchal,[1] Anuradha Gopalan,[4] Juan Zurita,[1] Samuel Achilefu,[9] Gabriela Chiosis,[1] Vladimir Ponomarev,[1] Markus Schwaiger,[7] Brett S. Carver,[3] Martin G. Pomper,[6] and Jan Grimm[1,2,10,11]

[1]Molecular Pharmacology Program, [2]Department of Radiology, [3]Human Oncology and Pathogenesis Program, and [4]Genitourinary Division, Department of Pathology, Memorial Sloan Kettering Cancer Center, New York, NY
[5]Gordon Center for Medical Imaging, Massachusetts General Hospital and Harvard Medical School, Boston, MA
[6]Russell H. Morgan Department of Radiology and Radiological Sciences, Johns Hopkins University, Baltimore, MD
[7]Department of Nuclear Medicine and [8]Department of Pathology, Technische Universität München, Klinikum rechts der Isar, Munich, Germany
[9]Department of Radiology, Washington University School of Medicine, St. Louis, MO
[10]Department of Pharmacology and [11]Department of Radiology, Weill Cornell Medical College, New York, NY

Prostate-specific membrane antigen (PSMA) or folate hydrolase 1 (FOLH1) is highly expressed on prostate cancer. Its expression correlates inversely with survival and increases with tumor grade. However, the biological role of PSMA has not been explored, and its role in prostate cancer remained elusive. Filling this gap, we demonstrate that in prostate cancer, PSMA initiates signaling upstream of PI3K through G protein–coupled receptors, specifically via the metabotropic glutamate receptor (mGluR). PSMA's carboxypeptidase activity releases glutamate from vitamin B9 and other glutamated substrates, which activate mGluR I. Activated mGluR I subsequently induces activation of phosphoinositide 3-kinase (PI3K) through phosphorylation of p110β independent of *PTEN* loss. The p110β isoform of PI3K plays a particularly important role in the pathogenesis of prostate cancer, but the origin of its activation was so far unknown. PSMA expression correlated with PI3K–Akt signaling in cells, animal models, and patients. We interrogated the activity of the PSMA–PI3K axis through positron emission tomography and magnetic resonance imaging. Inhibition of PSMA in preclinical models inhibited PI3K signaling and promoted tumor regression. Our data present a novel oncogenic signaling role of PSMA that can be exploited for therapy and interrogated with imaging.

INTRODUCTION

Prostate cancer is the most common cancer diagnosed in men. It is estimated that one in every seven men will be diagnosed with the disease during his lifetime. Although the medical community utilizes early diagnostic tools and new therapeutic approaches for localized disease, the National Institutes of Health's Surveillance, Epidemiology, and End Results Program (SEER) estimates that 26,730 deaths will be attributed to metastatic prostate cancer in 2017. Molecular hallmarks of prostate cancer include aberrant signaling of the androgen receptor (AR) and phosphoinositide 3-kinase (PI3K) pathways (Ferté et al., 2010; Perner et al., 2015), as well as expression of prostate-specific membrane antigen (PSMA; Sweat et al., 1998). In fact, PSMA (also known as folate hydrolase 1 [FOLH1] or glutamate carboxypeptidase II [GCPII]; EC number 3.4.17.21; gene symbol FOLH1; gene ID 2346) is the most prominent pros-

tate cancer cell-surface biomarker and is also found in the neovasculature of solid tumors (Chang et al., 1999). PSMA (FOLH1, GCPII) is normally expressed in the proximal renal tubules and duodenum, where it plays a major role in the processing and uptake of dietary folates, and in the brain, where it processes *N*-acetyl-ʟ-aspartyl-ʟ-glutamate (NAAG) to modulate the output of glutamate signaling transduced via the metabotropic glutamate receptor (mGluR) pathway (Rajasekaran et al., 2005; Rahn et al., 2012a). PSMA has been successfully used for the imaging of primary and metastatic prostate cancer in patients with radiolabeled PSMA-targeting antibodies or, more recently, small molecules (Pandit-Taskar et al., 2015; Maurer et al., 2016). PSMA-targeted radiotherapy in metastatic castration-resistant prostate cancer was recently able to confer

improved biochemical and radiological response, with sustained decline in prostate-specific antigen (PSA) levels and decreased lesion number and size (Kratochwil et al., 2016; Rahbar et al., 2017). In spite of the significant interest in PSMA as a target for imaging and therapy, the biological role of PSMA in prostate cancer remained elusive. Although previous studies showed that PSMA confers an advantage to prostate cancer cells through the processing of polyglutamated folates to folic acid and additionally affects the expression of proinflammatory cytokines (Yao and Bacich, 2006; Colombatti et al., 2009), an exact mechanism explaining a biological function of PSMA in prostate cancer was until now not known. In this work, we demonstrate that PSMA activates PI3K–Akt signaling in prostate cancer through release of glutamate as messenger molecule.

In addition to using PSMA as a structural anchor for targeted radiotherapeutics or experimental drugs (Hrkach et al., 2012), the primary clinical management of prostate cancer is currently based on therapeutic interventions that target the AR cascade, including androgen deprivation, antiandrogens, and neoadjuvant chemotherapy (Mitsiades, 2013). Unfortunately, patients almost always stop responding to AR inhibitors within 6 to 12 mo and progress to castration-resistant prostate cancer (Yuan et al., 2014). Genomic studies revealed that 40% of primary and 70% of metastatic prostate cancer patients have alterations in the PI3K signaling axis, including loss of *PTEN*, which along with the AR support survival signals in the disease (El Sheikh et al., 2008; Reid et al., 2010; Taylor et al., 2010). Particularly, it was shown that PI3K signaling in prostate cancer depends predominantly on PI3K's p110β isoform (Jia et al., 2008; Jiang et al., 2010). However, the mechanism of p110β activation in prostate cancer remained so far unknown (Schwartz et al., 2015). Efforts to elucidate this key mechanism demonstrated p110β activation by a G protein–coupled receptor (GPCR; Cizmecioglu et al., 2016), but the exact GPCR remained unknown. In our work, we show that PSMA activates a GPCR (mGluR I) through release of glutamate. Up-regulation of mGluR's expression has been identified in several malignancies, including prostate cancer (Yu et al., 2017). The findings of this study propose the use of PSMA as a surrogate marker for the activity of the PI3K signaling axis, which can be interrogated through molecular imaging with positron emission tomography (PET) imaging.

Combination therapies that block AR and PI3K pathways have been proposed. However, therapy with PI3K inhibitors in a disease-specific fashion has been challenging because of toxicity issues associated with off-tumor side effects from suppression of PI3K signaling in healthy organs (Dienstmann et al., 2014). In this work, we demonstrate that PSMA activates PI3K–Akt signaling in prostate cancer and demonstrate a new combination therapy in the inhibition of AR and PSMA as an alternative, tumor-selective strategy for PI3K signaling suppression to avoid PI3K inhibition in healthy tissues that lack PSMA expression.

RESULTS

Expression of PSMA in patients with prostate cancer correlates with elevated mTOR signaling

Because PSMA (FOLH1) has been identified as a promising marker for prostate cancer, we investigated whether its expression is reflective of disease state in cancer patients. We first analyzed genomic data obtained from prostate cancer patients with localized disease at our institution, and we found that higher PSMA expression was positively associated with faster biochemical recurrence (Fig. 1 A and Table S1) and metastasis (Fig. 1 B and Table S2). Given the clear correlation of PSMA with disease aggressiveness, we examined whether overexpression of PSMA correlates with alterations in major oncogenic signaling pathways. Immunohistochemical analysis of tissue microarray samples of prostate cancer patients showed that increased PSMA levels are indeed associated with the phosphorylation of 4EBP1, a downstream target of the mammalian target of rapamycin (mTOR; Fig. 1 C). Subsequent gene set enrichment analysis of patients' genomics data further corroborated the histopathological findings, revealing that PSMA levels are associated with changes in the transcriptional levels of mTOR-regulated genes (Fig. 1 D). Collectively, these observations in clinical samples of prostate cancer prompted us to further elucidate a possible PSMA-induced signaling mechanism, which may provide novel personalized therapeutic interventions with improved disease management through PSMA-targeted PET imaging.

PSMA promotes downstream Akt signaling in prostate cancer

Intrigued by the clinical findings, we next examined whether PSMA expression in prostate cancer cell lines has any effect on the Akt–mTOR signaling cascade. To achieve this, we used human prostate cancer cell lines, which either expressed (LNCaP-Ctrl and PC3-PSMA) or lacked PSMA (LNCaP-KD and PC3-Ctrl; Fig. S1, A–C). Gene set enrichment analysis revealed that in cells expressing PSMA, the levels of genes involved and regulated by Akt and mTOR were elevated (Fig. 2 A), similar to what was observed in patients, indicating that PSMA modulates the activity of the Akt–mTOR cascade in prostate cancer.

Because the PSMA protein itself does not carry any signaling-relevant moieties, we then focused on its enzymatic function as a glutamate carboxypeptidase. In the brain, PSMA modulates neuronal signaling within the synaptic cleft by hydrolyzing the amide bond that links the glutamate moiety with *N*-acetylaspartate of the neurotransmitter NAAG. The released glutamate then activates postsynaptic metabotropic glutamate receptors, leading to mobilization of calcium within the postsynaptic neuron (Fig. 2 B). We reasoned that a similar mechanism might be at play in prostate cancer cells as well. Specifically, we examined whether similar to its function in the brain PSMA's enzymatic release of glutamate could activate mGluR to facilitate activation of the PI3K–Akt–mTOR axis. Because PSMA is known to hydrolyze folic
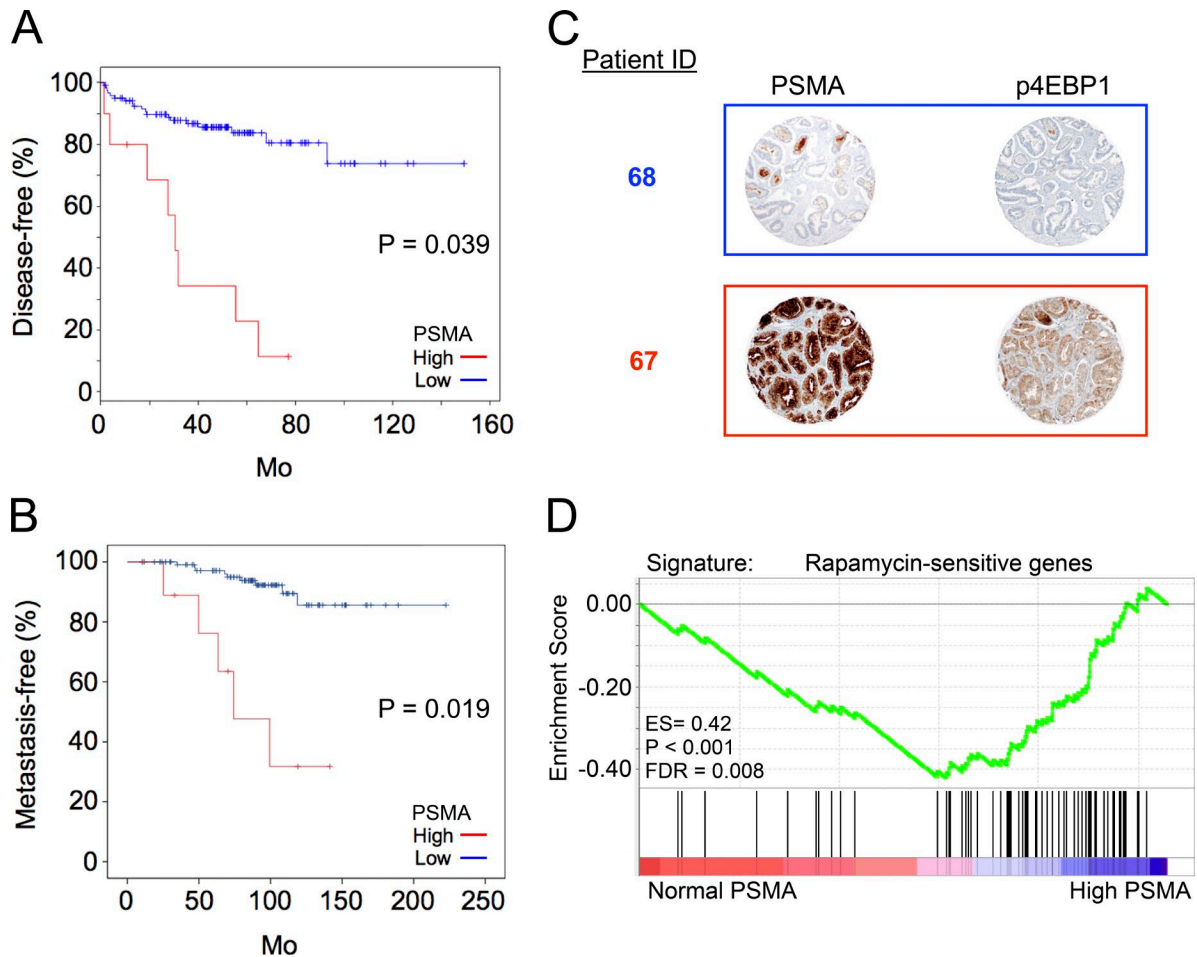
Figure 1. **Expression of PSMA in patients is associated with activated Akt.** (A and B) Elevated PSMA expression is associated with disease relapse (A) and metastases (B) in prostate cancer (MSKCC cohort PMID 25024180). High PSMA expression is defined as expression z-score >2, and low PSMA expression is defined as z-score ≤ 2. (C) Immunohistochemistry on representative samples from prostate cancer patients shows that enhanced PSMA expression correlates with elevated phosphorylation of the Akt target 4EBP1. (D) Gene set enrichment analysis comparing prostate cancer patients with normal PSMA levels with prostate cancer patients with high (z-score >2) PSMA levels. The dataset from the MSKCC prostate cancer cohort (PMID 25024180) was used.

acids (Yao et al., 2008), we replaced NAAG for folic acid (vitamin B9) as PSMA substrate, because vitamin B9 is ubiquitous in the body. Toward this direction, we first confirmed the transcriptomic findings by assessing the phosphorylation levels of Akt and its downstream targets. Indeed, we found that expression of PSMA increased the phosphorylation of Akt and its downstream targets S6K and 4EBP1, whereas ablation of PSMA expression had the opposite effect (Fig. 2, C–F). Inhibition of PSMA's enzymatic activity with the highly selective inhibitor 2-PMPA (Zhou et al., 2005; K_i = 275 pM) resulted in a decrease in phosphorylation (Fig. 2 G), which was comparable to suppression of PSMA expression. Having demonstrated that PSMA activates Akt–mTOR signaling through its enzymatic activity, we next determined whether PSMA could be a bona fide modulator of oncogenic signaling in prostate cancer. Therefore, we engineered PC3 cells to express enzymatically active PSMA (PC3-PSMA$_{wt}$), and

implanted them in male, athymic nude mice. Immunohistochemistry on slices from mouse xenografts showed that expression of wild-type PSMA was associated with elevated Akt phosphorylation (Fig. 3 A and Fig. S1, D–G), which was in line with our in vitro studies and clinical findings. These data show that PSMA expression in prostate cancer up-regulates the Akt–mTOR signaling pathway and is mediated through PSMA's enzymatic activity.

PSMA controls the phosphorylation of p110β, but not p110α or p110δ

As the PI3K-p110β isoform is particularly implicated in prostate cancer (Jia et al., 2008; Jiang et al., 2010), and because p110β is probably activated by a yet-unknown GPCR (Cizmecioglu et al., 2016), we hypothesized that glutamate released by PSMA may activate PI3K in an isoform-specific mode through the GPCRs of the mGluR I group. To test
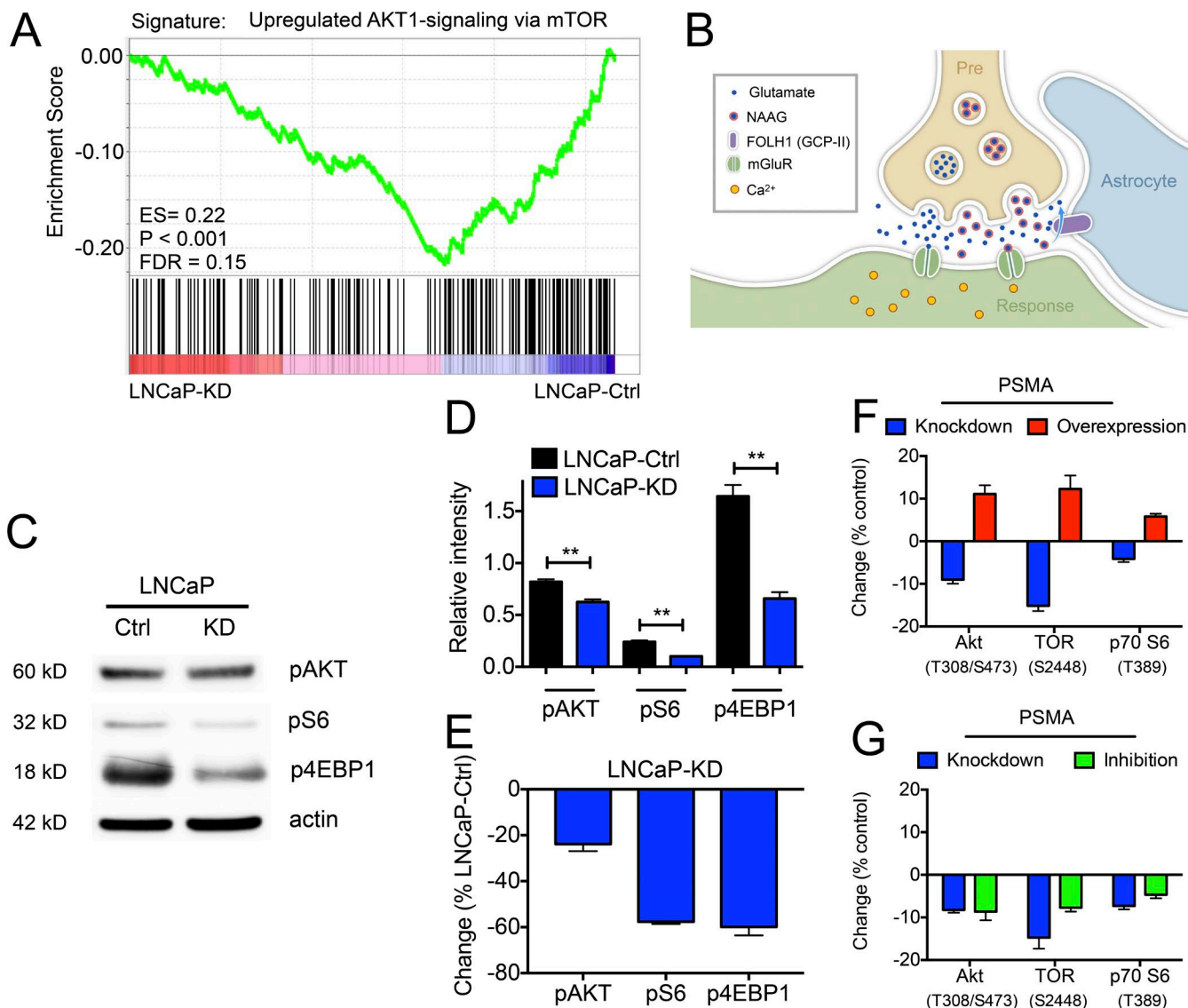
Figure 2. **Expression of enzymatically active PSMA up-regulates the Akt–mTOR pathway.** (A) PSMA-expressing cells are associated with enrichment of Akt and mTOR signaling signatures. Gene set enrichment analysis comparing PSMA-expressing cells (LNCaP-Ctrl) with their PSMA-negative counterparts (LNCaP-KD). The gene set data were derived from the mean of three independent experiments obtained through the Affymetrix platform. (B) In the brain, PSMA, encoded by the FOLH1 gene and termed glutamate carboxypeptidase II (GCP-II), modulates glutamatergic neurotransmission via activation of post-synaptic metabotropic glutamate receptor (mGluR) system through the proteolytic cleavage of the amide bond of NAAG. (C–E) Increased phosphorylation of Akt, S6, and 4EBP1 in PSMA-expressing cells was determined with immunoblot analysis. Relative intensities normalized to actin levels ($n = 3$). (F and G) Expression of enzymatically active PSMA leads to phosphorylation of Akt, mTOR, and S6, as determined through a reverse-phase protein array (R&D Systems, Inc.). Changes in phosphorylation calculated as deviations from the control cell line (LNCaP-Ctrl for the PSMA knockdown cells [LNCaP-KD], PC3-Ctrl for PC3-PSMA that overexpress PSMA, and LNCaP-Ctrl for LNCaP-Ctrl cells that were treated for 2 h with the PSMA inhibitor 2-PMPA; $n = 4$ per condition). Graphs show mean ± SEM. **, $P < 0.01$ (unpaired t test).

this, we used a clinically translational proteomics platform with high-throughput capabilities that utilizes as few as 25 cells and examines the global phosphorylation status of the protein of interest through changes of the proteins isoelectric point (NanoPro 1000; Protein Simple). We identified that inhibition of PSMA's enzymatic activity impaired phosphorylation of PI3K-p110β, but not the p110α and p110δ isoforms (Fig. 3 B). Importantly, control treatment with an mGluR I agonist resulted in phosphorylation of p110β only similar to activation by PSMA in the presence of glutamated folate. Control studies corroborated that inhibition of p110β in prostate cancer decreased the phosphorylation of Akt (Fig. 3 C and Fig. S2 A), whereas glutamated folate did not alter the activation of Akt in cells lacking PSMA (Fig. S2 B).
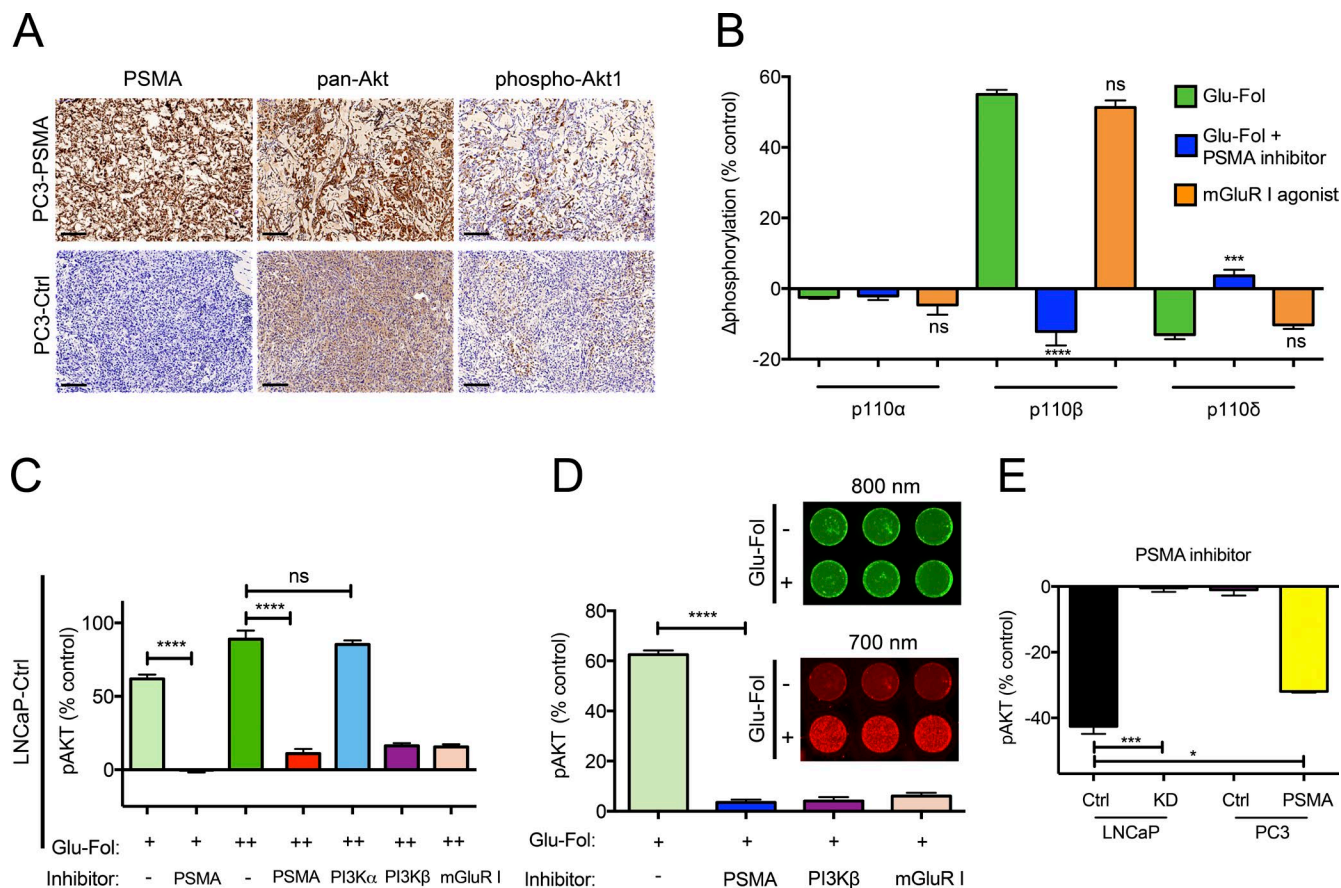
Figure 3. **PSMA up–regulates Akt through activation of PI3K–p110β via mGluR I.** (A) Immunohistochemistry of PC3-Ctrl and PC3-PSMA tumors grown on male, athymic nude mice shows elevated Akt1 phosphorylation in the PSMA-expressing tumors. Representative images of slices fixed in paraffin and stained with anti–human PSMA, pan-Akt, and phospho-Akt1 antibodies (bars, 100 µm). (B) Global changes in the phosphorylation status of components of the PI3K pathway were determined with the NanoPro 1000 system (Protein Simple). NanoPro-based analysis of PI3K's catalytic subunits in LNCaP-Ctrl cells following 2 h stimulation with monoglutamated folate (Glu-Fol) or an mGluR I agonist (L-Quisqualic acid; PSMA inhibitor: 2-PMPA) in basal medium deprived of serum, folate and glutamate, showing that PSMA facilitates the phosphorylation of PI3K-p110β though activation of mGluR I. Before stimulation, the cells were starved for 24 h in basal medium. Phosphorylation alterations were calculated as the difference observed between the treatment group and unstimulated cells (n = 3 per condition). (C) Inhibition of PI3K-p110β suppresses Akt activation, similar to PSMA and mGluR I inhibition in prostate cancer. LNCaP-Ctrl cells were treated with Glu-Fol and inhibitors for 2 h. Phosphorylation was assessed through a reverse-phase protein array (n = 3 per treatment). (D) The fluorescent Akt-specific substrate LS456, whose fluorescence emission shifts from emission in the near-infrared range (λ = 800 nm) to the red sector of the visible light (λ = 700 nm) upon phosphorylation by the kinase, was used to assess Akt activation by PSMA. LNCaP-Ctrl cells were treated with Glu-Fol and pharmacological agents for 2 h, as described above for panel B of this figure (n = 12 per treatment). (E) Inhibition of PSMA's enzymatic activity with 2-PMPA decreases Akt's phosphorylation in PSMA-expressing cells. Cells were grown in complete medium and treated for 2 h with 2-PMPA. Control cells were treated with 1× PBS. Changes in Akt's phosphorylation were determined with a reverse-phase protein array (n = 3 per treatment). Graphs show mean ± SEM. ns, not significant; *, $P < 0.05$; ***, $P < 0.001$; ****, $P < 0.0001$ (ordinary one-way ANOVA).

To further confirm that PSMA specifically activates p110β in prostate cancer, we used an Akt-specific fluorescent substrate that emits at 700 nm once phosphorylated by Akt (Shen et al., 2013) and observed that inhibition of PSMA, mGluR I, or p110β equally suppressed Akt activation (Fig. 3 D). Through a reverse-phase protein array, we observed that inhibition of PSMA's enzymatic activity in PSMA–expressing cells decreased Akt activation but had no effect in cells lacking PSMA (LNCaP-KD and PC3-Ctrl; Fig. 3 E). Next, in order to corroborate that it really is the enzymatic activity of PSMA that induces the signaling cas-

cade, we created cells that expressed enzymatically inactive PSMA (PC3-PSMA_mut). In these cells glutamated folate did not induce activation of Akt or its downstream targets, such as PRAS40 (Fig. S2, C–E). We also determined that in prostate cancer cells that have wild–type, functional PTEN and express PSMA (22Rv1), treatment with glutamate folate induced activation of Akt, similar to PSMA-expressing cells that do not express PTEN (LNCaP; Fig. S2, F–K). Furthermore, inhibition of PSMA decreased the activity of the Akt-target epithelial nitric oxide synthase and increased that of the AR, as reflected in higher levels of the PSA (Fig. S2, L and M).
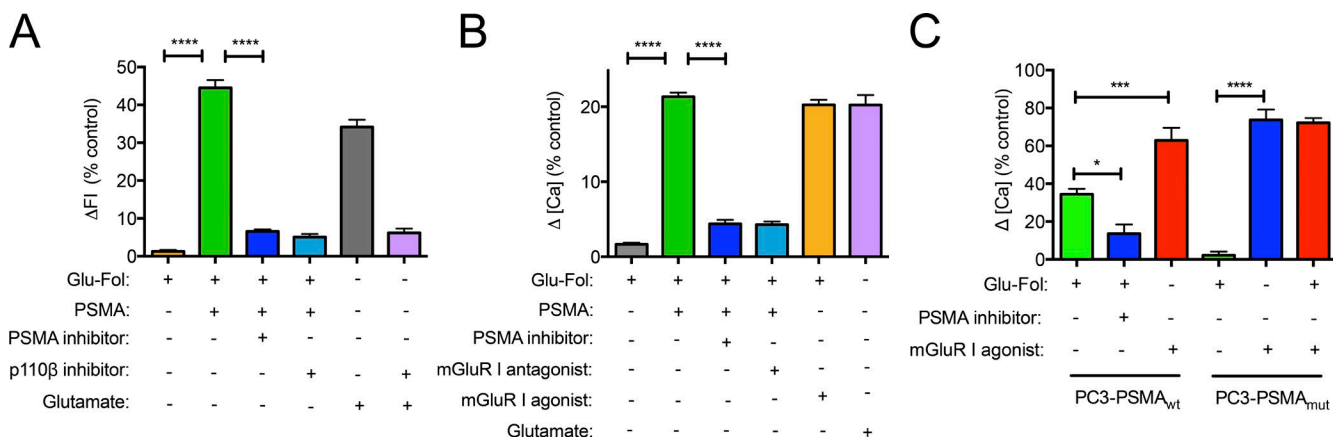
Figure 4. Released glutamate from PSMA–processed glutamate folate activates mGluR I and up–regulates cytoplasmic calcium levels. (A) PSMA activates Akt in a p110b-dependent fashion, using glutamate as the molecular messenger. PC3-Ctrl cells grown on 96-well plates were supplemented with Glu-Fol, recombinant PSMA, and inhibitors for 2 h. The change in 700-nm fluorescence intensity emission of the Akt-specific substrate LS456 was calculated based on unstimulated cells ($n = 12$ per treatment). (B) The released glutamate by PSMA engages mGluR I, mobilizing calcium to the cytoplasm. PC3-Ctrl cells were incubated in basal medium deprived of serum, folate, and glutamate for 4 h at 37°C, 5% CO_2 (mGluR I agonist: (S)-3,5,-DHPG; $n = 8$ per condition). Detection was achieved with the Fluo-4 Direct calcium kit. (C) Intracellular calcium levels upon stimulation of cells expressing wild-type ($PSMA_{wt}$) and enzymatically inactive PSMA ($PSMA_{mut}$). Changes in $[Ca^{2+}]$ were calculated with respect to nonstimulated PC3-$PSMA_{wt}$ or PC3-$PSMA_{mut}$ cells grown in basal RPMI medium, as mentioned above for panel B of this figure (mGluR I agonist: (S)-3,5,-DHPG; $n = 8$ per condition). Graphs show mean ± SEM. *, $P < 0.05$, ***, $P < 0.001$; ****, $P < 0.0001$ (ordinary one-way ANOVA).

This is in line with previous work that demonstrated that inhibition of PI3K releases inhibition of the AR, and vice versa (Carver et al., 2011). Because of the elevated activity of Akt and epithelial nitric oxide synthase, it is likely possible that the higher levels of Akt protein in PSMA-expressing tumors (Fig. 3 A and Fig. S1 E) might be due to nitric oxide up-regulating the transcription factor RUNX2, which regulates expression of Akt, in a reciprocal feedback loop in prostate cancer (Cohen-Solal et al., 2015; Nesbitt et al., 2016). Collectively, these data demonstrate that through its ability to hydrolyze glutamated folates, PSMA facilitates activation of PI3K-p110β and Akt via mGluR I, thus promoting oncogenic signaling in prostate cancer. Collectively, these data show that PSMA activates p110β through enzymatic release of glutamate from folic acid.

PSMA activates mGluR I through the release of glutamate

After showing that PSMA initiates p110β-dependent PI3K signaling via mGluR I as a result of its enzymatic release of glutamate from glutamated folate, we further evaluated the consequences of PSMA-mediated activation of the GPCR mGluR I. Outside the central nervous system, such as in the duodenum, PSMA similarly releases free glutamate from glutamated folates through its zinc metalloproteinase catalytic mechanism (Klusák et al., 2009). We therefore showed that exogenous supplementation of the culture medium with either free glutamate or glutamated folate and recombinant PSMA activated Akt in a p110β-specific mode in PSMA-negative cells (Fig. 4 A).

Because PSMA regulates calcium levels in the brain through the release of glutamate, we reasoned that PSMA could also regulate calcium-mediated signaling in prostate cancer. Hence, we examined whether PSMA's processing of glutamated folates had an impact on phospholipase C activation and cytoplasmic calcium levels in prostate cancer. In line with our proposed mechanism, elevation of cytoplasmic calcium was observed in PSMA-expressing cells in the presence of glutamated folates in a dose-dependent pattern (Fig. S3, A–C). Supplementation of PSMA-null cells with glutamated folate and recombinant PSMA caused calcium increase in the cytoplasm, which was inhibited in the presence of either 2-PMPA or the mGluR I antagonist (Fig. 4 B).

In PSMA-expressing cells, treatment with an mGluR I antagonist, phospholipase C inhibitor, or 2-PMPA abrogated the PSMA-mediated calcium influx to the cytoplasm, whereas mGluR I agonists potentiated it (Fig. S3 D). These findings indicate that PSMA-triggered mGluR I activation also leads to phospholipase C activation and downstream activation of inositol trisphosphate receptors that release calcium from the endoplasmic reticulum to the cytoplasm. Because apart from mGluR I, calcium levels can be also modulated by NMDA and AMPA receptors, we treated PSMA-expressing cells with inhibitors of these receptors. We found that treatment with these compounds did not have any effect on calcium levels in the presence of glutamated folate (Fig. S3 E), demonstrating that mGluR I is activated by free glutamate released by PSMA at the plasma membrane of prostate cancer cells. Because treatment with an mGluR I agonist caused calcium mobilization in cells lacking PSMA, this showed that the glutamatergic system was functional in these cells (Fig. S3 F). As cells expressing PSMA had also higher
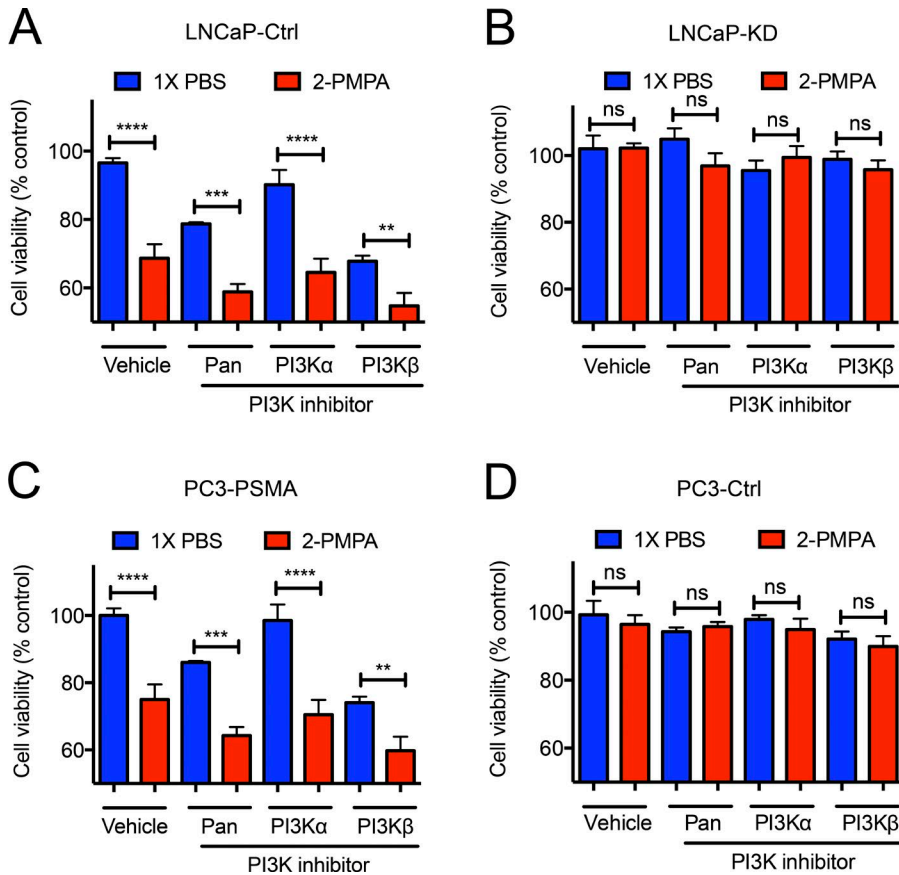
Figure 5. Inhibition of PSMA improves response to chemotherapy in vitro. (A–D) Inhibition of FOLH's enzymatic activity and PI3K-p110β reduces the viability of PSMA-expressing prostate cancer cells. Cells were treated with PI3K inhibitors (Pan: BKM120; PI3Kα: BYL719; PI3Kβ: GSK2636771; [inhibitor] = 200 nM) and 2-PMPA (200 nM) for 48 h at 37°C, 5% CO_2 (n = 12 per treatment). Viability was determined with the Alamar blue assay. Graphs show means ± SEM. ns, not significant; **, P < 0.01; ***, P < 0.001; ****, P < 0.0001 (ordinary one-way ANOVA).

total calcium content than cells lacking this enzyme (Fig. S3 G), this indicates that prostate cancer may rapidly mobilize calcium from the endoplasmic reticulum to the cytoplasm for signal transduction. Inhibition of PSMA's enzymatic activity decreased the levels of inositol trisphosphate (Fig. S3 H), demonstrating that PSMA may have first stimulated mGluR I at the plasma membrane via glutamate, which in turn triggered phospholipase C to generate inositol trisphosphate that activated endoplasmic reticulum's inositol trisphosphate receptors to release calcium to the cytosol. Indeed, activation of mGluR I and initiation of downstream cytoplasmic calcium efflux is mediated by PSMA at the plasma membrane, where PSMA colocalized tightly with the two members that constitute the mGluR I family (mGluR1 and mGluR5; Fig. S3 I). Hence, in order to relay environmental and nutrient cues to intracellular oncogenic signals using calcium as secondary messenger, PSMA at the plasma membrane has to be enzymatically active, as expression of enzymatically inactive PSMA (Ghosh and Heston, 2003) abolished calcium mobilization in the presence of glutamated folate, whereas mGluR I was still functional (Fig. 4 C and Fig. S3 J). Overall, these data show that PSMA uses glutamated folate as its substrate for the production of glutamate that will locally activate mGluR I, leading to downstream signaling that supports prostate cancer progression.

Inhibition of PSMA in vivo confers a therapeutic advantage

Having demonstrated that expression of PSMA in prostate cancer patients is associated with Akt activation and faster disease progression and that PSMA through its enzymatic activity activates the PI3K–Akt axis, we next evaluated whether targeting of PSMA could serve as potential pharmacological treatment avenue. Given that new targeted therapies are on the rise, we identified that PSMA inhibition improved the effect of PI3K and mTOR inhibitors in vitro (Fig. 5, A–D; and Fig. S4, A and B). Because the PSMA inhibitor 2-PMPA has been previously used in clinical studies as a neuroprotective agent for diseases like multiple sclerosis (Zhou et al., 2005; Rahn et al., 2012b), we used it to prime animals that had PSMA-expressing xenografts and observed reduced tumor volume and growth (Fig. 6, A–C; and Fig. S5, A–I). Importantly, dose escalation further decreased tumor growth in animals with PSMA-positive xenografts (Fig. S5 J), and ablation of PSMA expression impaired tumor growth (Fig. S5, K–M).

Because PSMA activates the PI3K pathway and the AR negatively regulates PI3K, we next asked whether concomitant inhibition of the AR pathway and PSMA-mediated activation of PI3K could improve treatment of PSMA-expressing tumors. We found that animals treated with either the anti-androgen enzalutamide or 2-PMPA had smaller tumors
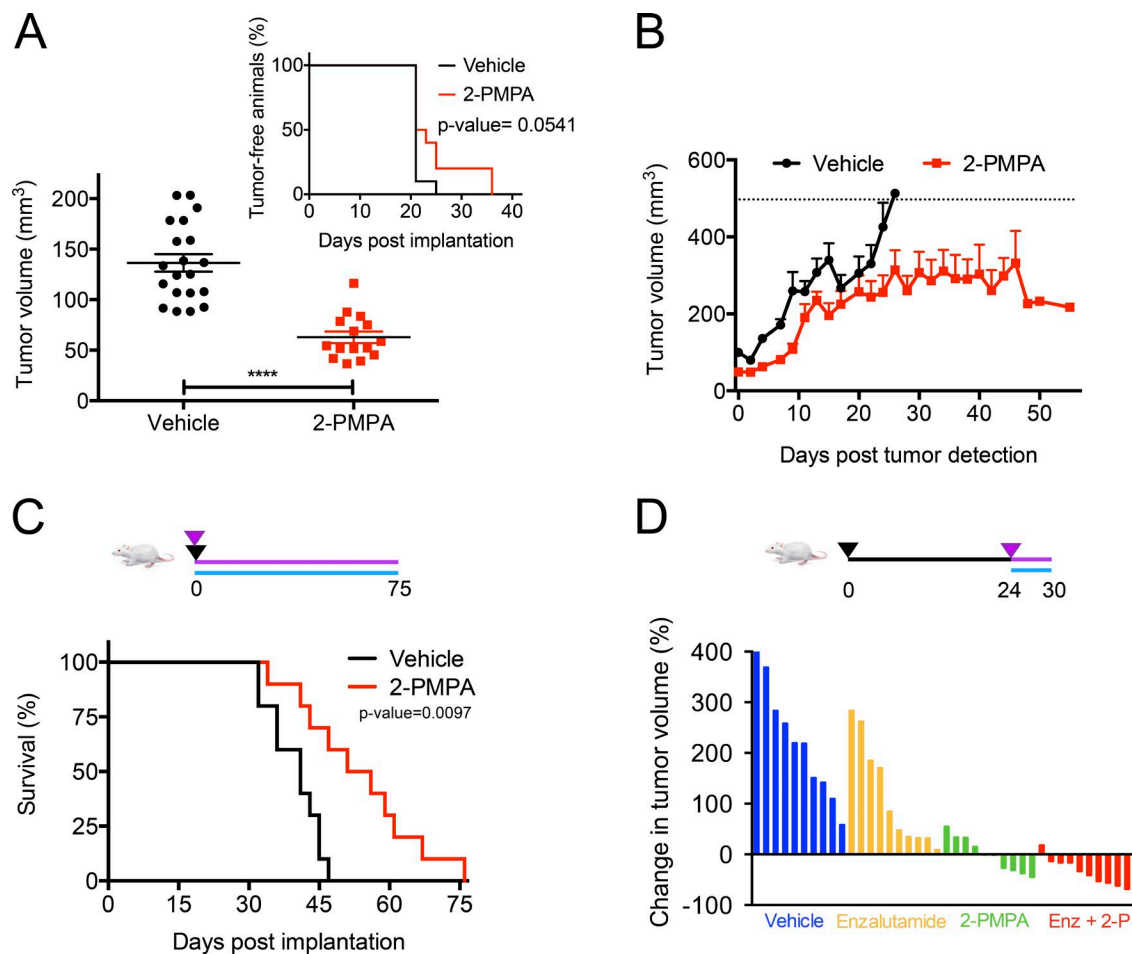
Figure 6. **Inhibition of PSMA's enzymatic activity in vivo provides a treatment benefit.** (A and B) Male, athymic nude mice with LNCaP-Ctrl xenografts on both of their flanks were treated daily with vehicle (1× PBS) or PSMA inhibitor (2-PMPA) administered i.v. immediately after implantation of the cells (n = 10 mice per cohort). Graphs show mean ± SEM. ****, P < 0.0001 (unpaired t test). Inset shows the day where the tumors were first detected (n = 10 mice per cohort). (C) Survival curves of mice bearing LNCaP-Ctrl xenografts on their flanks (n = 10 animals per cohort). The animals received daily i.v. treatment (vehicle: 1× PBS; PSMA inhibitor: 2-PMPA) during the course of the study (75 d after implantation; day 0, implantation day). p-value was determined using the Gehan–Breslow–Wilcoxon test. (D) Waterfall plot of animals having bilateral LNCaP-Ctrl xenografts on their flanks (n = 5 mice per group). Treatment was administered daily i.v. on day 24 after xenograft implantation (enzalutamide, 0.5 mg/kg; 2-PMPA, 20 mg/kg; Enz + 2-P, 0.5 mg/kg enzalutamide and 20 mg/kg 2-PMPA). The black arrowhead on the timelines of C and D indicates the day of xenograft implantation, the purple arrowhead the day treatment started, the purple line the length of treatment, and the continuous blue line that the treatment was daily.

than control animals (Fig. 6 D). However, marked regression was observed in animals that received the antiandrogen and PSMA inhibitor, where the volume of 9 out of 10 tumors decreased (0 out of 10 tumors regressed with enzalutamide alone, and 4 out of 10 tumors treated with 2-PMPA decreased; Fig. 6 D and Fig. S5 N, inset). Combination therapy with enzalutamide and an mGluR I antagonist indeed conferred a therapeutic benefit, although it was less effective because of the poor aqueous solubility and stability of the mGluR I antagonist (Fig. S5 N). We further confirmed that treatment with 2-PMPA did not affect the growth of xenografts lacking PSMA that were implanted in $PSMA^{+/+}$ or $PSMA^{-/-}$ animals (Fig. S5, O and P), indicating that the inhibitor's therapeutic effect is associated with inhibition of the enzymatic activity

of tumor-expressed PSMA. Overall, these data further suggest that inhibition of PSMA in vivo may confer a therapeutic benefit, where by targeting the tumor's PSMA, its PI3K signaling is suppressed and off-tumor–associated toxicities caused by PI3K signaling inhibition are averted.

PSMA expression in prostate cancer patients correlates with Akt activity

After showing that PSMA inhibition provides a therapy benefit and that PSMA activates p110β–dependent Akt signaling, and because prior work has identified PSMA as a promising biomarker for prostate cancer, we investigated whether PSMA expression was associated with distinct molecular profiles in patients, allowing stratification toward personalized, precision

medicine. Therefore, we screened a tissue microarray consisting of samples from 76 prostate cancer patients and found that expression of PSMA correlates with phosphorylation of the Akt target 4EBP1 (Fig. 7 A and Fig. S4, C–H). PTEN's levels did not correlate with PSMA levels and 4EBP1 status (Fig. S4 F). These findings prompted us to examine whether noninvasive assessment of PSMA expression through PET imaging could predict Akt activation in patients and thus serve as a potential prognostic marker that guides therapy. We examined whether Akt phosphorylation is higher in patients with elevated PSMA levels, determined noninvasively with PET and magnetic resonance imaging (MRI) and the PSMA-specific probe ^{68}Ga-HBED-CC before prostatectomy (Eder et al., 2012; Maurer et al., 2016). After prostatectomy, sections of the removed tumor underwent histopathological analysis, including quantitative immunofluorescence microscopy for PSMA and phosphorylated Akt, in order to obtain global tumor molecular information and address disease heterogeneity issues (Fig. 7, B and C). Principal component analysis (PCA) identified that PSMA expression and tracer uptake more strongly correlated with Akt's phosphorylation at S473 than other clinical indicators of prostate cancer, such as Gleason score and PSA (Fig. 7, D and E). Despite the variability among samples from each patient (which is common because of cancer's heterogeneity), these findings show that PSMA-based PET imaging can serve as a predictor of the global activation status of the PI3K–Akt pathway in a prostatic lesion. Particularly when grading nearly identical tumors, this will provide a new means of risk stratification for patients and help identify those patients that require more aggressive therapy.

DISCUSSION

Patient stratification has long been sought for treatment optimization of men with primary and metastatic prostate cancer. The carboxypeptidase PSMA, which is strongly expressed on prostate cancer, has been used increasingly as target to guide therapy and imaging agents to prostate cancer, yet its biological role in the disease remained elusive and unexplored. Using transcriptomics, proteomics, and imaging, we show for the first time that PSMA provides a signaling function by releasing glutamate from folic acid (vitamin B9). The glutamate activates nearby metabotropic glutamate receptors. These GCPRs lead to activation of p110β and concomitantly negatively regulate the AR pathway. Critical to signaling initiation is PSMA's processing of glutamated substrates, which activate proximal mGluR I, reminiscent of the enzyme's function within the synaptic clefts of the central nervous system. This indicates also that the vitamin B9 (folic acid) is a potential accelerator of prostate cancer, because it provides glutamate through PSMA. Importantly, a recent large study of almost 15,000 men showed that individuals with higher blood folate levels were at greater risk of high-grade prostate cancer (Price et al., 2016), underscoring the importance of our work.

Previous studies have shown that Akt signaling in prostate cancer is driven by the p110β isoform of PI3K by an unidentified GPCR (Jia et al., 2008). In line with this, it was demonstrated that inhibition of p110β confers a therapeutic advantage in vivo and that combination therapy with PI3K and AR inhibitors suppresses the reciprocal negative feedback loop between these two pivotal signaling axes in prostate cancer (Carver et al., 2011). However, to our knowledge, there have been no efforts to identify the mechanism by which a GPCR specifically activates p110β in animal models and prostate cancer patients. Prior work has shown that PSMA is overexpressed in prostatic neoplasias and that AR inhibition up-regulates PSMA levels (Evans et al., 2011). Additionally, PSMA was identified as a zinc metalloproteinase capable of processing glutamated folates, with the released folate providing a proliferative advantage to prostate cancer cells (Yao and Bacich, 2006; Klusák et al., 2009). Before these studies, the field of neuroscience provided evidence that the enzyme's role in the central nervous system is to modulate excitatory signaling through the processing of NAAG with refined spatiotemporal regulation. Different groups implied that the spatial regulation of PSMA at the plasma membrane might facilitate oncogenic signaling in prostate cancer, although the mechanism remained elusive (Rajasekaran et al., 2005; Colombatti et al., 2009). Our findings bridge this significant gap in knowledge and experimentally show that PSMA colocalizes with mGluR I members on the plasma membrane of prostate cancer cells, providing a mechanistic link between PSMA and mGluR I as the participating GPCR that activates p110β signaling. The causality between PSMA enzymatic activity and p110β-driven Akt signaling shown by our work provides an appealing justification for the β-isoform–specific induction of PI3K signaling in prostate cancer, irrespective of PTEN status, and establishes a central functional role of PSMA as a diagnostic and therapeutic target for the inhibition of GPCR-driven oncogenesis in cancer. Collectively, our data support the hypothesis that PSMA converts environmental signals, such as nutrient abundance, into proliferative signals that drive pro-oncogenic activities during prostate cancer.

Our findings have important clinical implications for prostate cancer patient treatment. Expression of PSMA correlates with activation of the PI3K–Akt pathway in patients. Noninvasive PET imaging can interrogate PSMA in the tumor with agents that are already in advanced clinical trials in the United States and Europe. Considering that the levels of PSA are not an accurate predictor of disease status and that prostate cancer is not FDG avid, our work suggests that PSMA-based PET imaging not only demonstrates the presence of prostate cancer but also noninvasively diagnoses a patient's underlying molecular signaling aberrations, providing improved patient stratification and better treatment. Because PSMA is expressed in the neovasculature of other solid tumors and many of these tumors coexpress members of the mGluR family (Ristau et al., 2014; Yu et al., 2017), our data argue that PSMA might additionally have similar function in the tumor neovasculature.
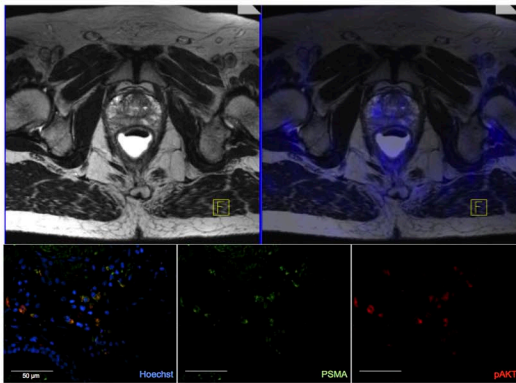
Lastly, the observation that PSMA activates the PI3K pathways and negatively regulates the AR pathway has sig-
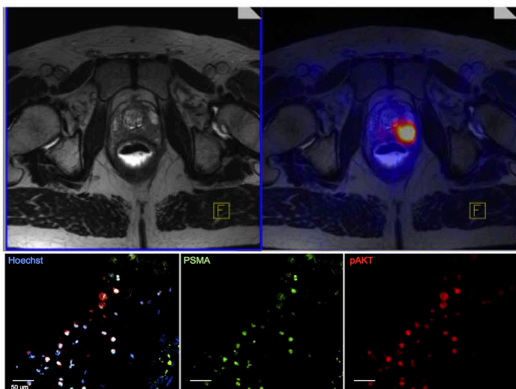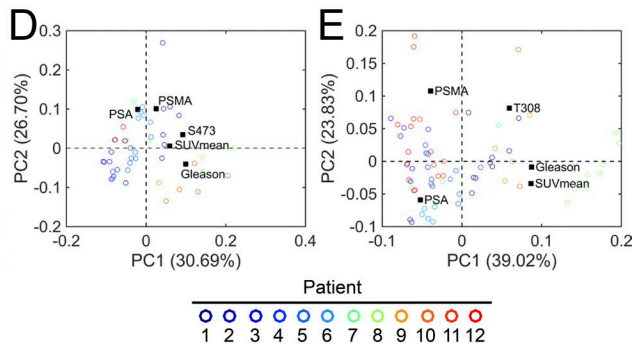
A

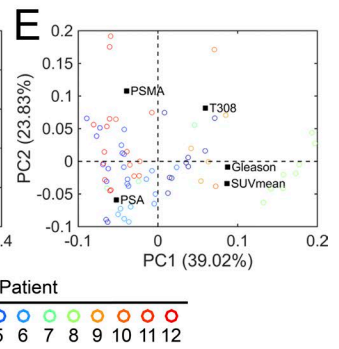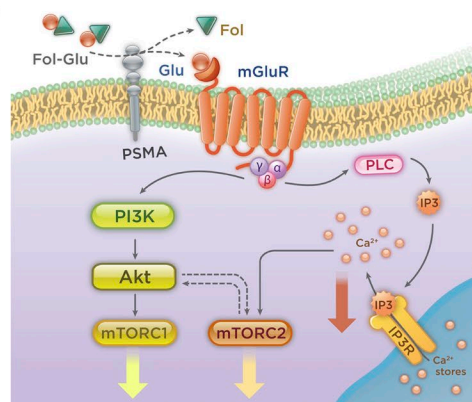|	PSMA	p4EBP1
Cluster A	Mixed	Moderate
Cluster B	High	Enhanced
Cluster C	Low	Low
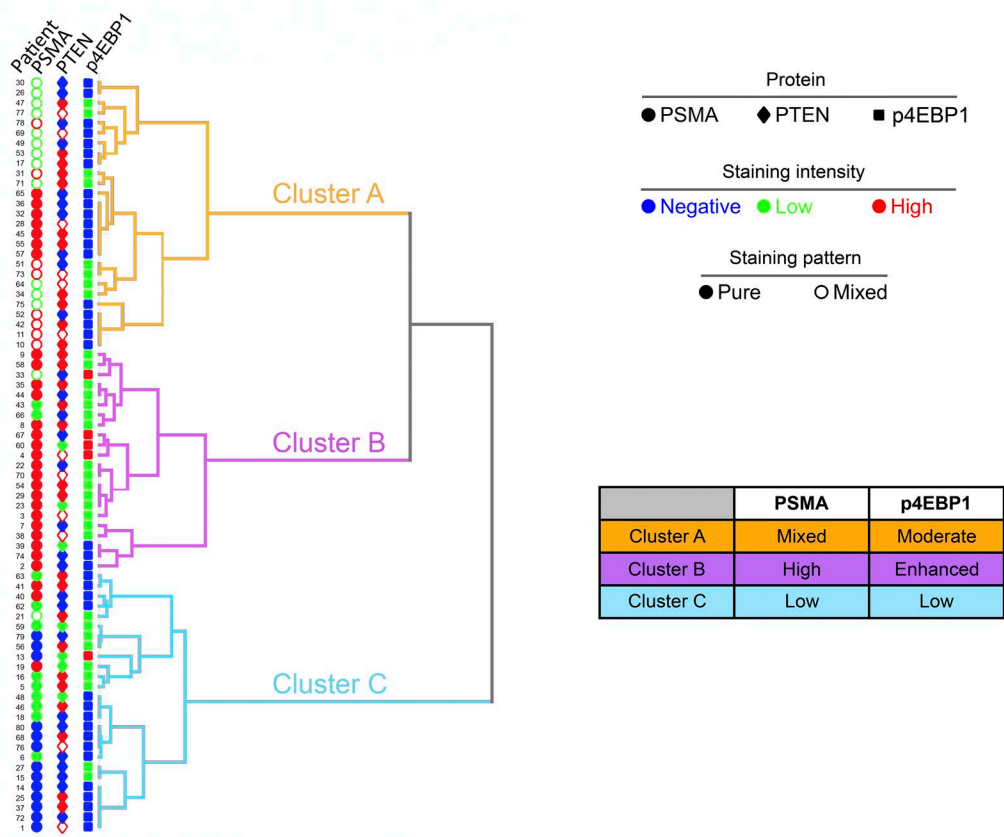
nificant clinical implications, because PSMA and mGluR I inhibitors could be used in tandem with antiandrogens, such as enzalutamide or abiraterone. Our work with preclinical inhibitors of mGluR I, such as NPS 2390, and the PSMA inhibitor 2-PMPA, which has been previously tested in the clinic, establish this combination therapy strategy in vitro and in vivo. Because prior work showed that the combination of inhibitors of the AR and PI3K is required to elicit therapeutic efficacy in prostate cancer (Carver et al., 2011), and that PI3K, Akt, or mTOR inhibitors have some limitations, including off-target effects caused by their constitutive expression in other organs, inhibition of PSMA can be an alternative therapeutic venue. In addition to pharmacological treatment, the results of the present study may provide dietary guidelines for cancer patients, such as folate-fortified food like bread and pasta (or frequently as an additive in Chinese food in the United States), and multivitamin supplements might support the pro-cancer activity of PSMA. It may also be intriguing if future studies delineate the temporal dynamics among PSMA-facilitated calcium mobilization, PI3K–Akt activation, and AR inhibition, along with evaluation of the status of PKC isozymes that are regulated by the AR in prostate cancer (Tanaka et al., 2003; Gonzalez-Guerrico et al., 2005; Xiao et al., 2009; Shankar et al., 2016) and control the activity of protein phosphatase 2, which modulates Akt.

In summary, our results demonstrate that apart from being a biomarker of prostate cancer, PSMA carries a previously unknown critical functional role in disease progression, transmitting environmental cues stemming from nutrients to initiate an intricate intracellular signaling repertoire. Specifically, through release of glutamate from glutamated folates, including vitamin B9, it activates the glutamatergic system, mobilizing calcium, activating PI3K (Fig. 7 F), and triggering a growth-prevailing cascade into the cell. As we have demonstrated, this provides new insights on disease dynamics, including the reason for the prevailing p110β signaling in prostate cancer, and therapeutic approaches, considering

that mGluR I is expressed in several cancers, including melanoma, lung, and pancreatic, and PSMA is expressed on the neovasculature of solid tumors. It is also possible that PSMA may up-regulate AKT activity via the calcium-dependent activation of mTORC2, which in turn can phosphorylate AKT (Huang et al., 2013; Josselyn and Frankland, 2013). This might suggest the presence of a positive feedback loop, which can be part of future investigational efforts. In conclusion, because several PSMA-specific imaging agents are entering the clinic and one in seven men will be diagnosed with prostate cancer, our findings may facilitate biology-based treatment planning toward precision oncology.

MATERIALS AND METHODS
Materials
Monoglutamate folate was purchased from Sigma-Aldrich, whereas the tri- and pentaglutamate folates were obtained from Schircks Laboratories. The following chemicals were acquired from Tocris: 2-PMPA (PSMA inhibitor), (S)-3,5,-DHPG (mGluR I agonist), L-quisqualic acid (mGluR I agonist), L-AP3 (mGluR I antagonist), U73122 (phospholipase C inhibitor), IEM 1460 (AMPAR blocker), D-AP5 (NMDA receptor antagonist), and NPS 2390 (mGluR I antagonist). From Sigma-Aldrich, we also obtained N-acetyl-L-cysteine and dimethyl sulfoxide. We purchased the following compounds from Selleck Chemicals: BKM120 (pan-PI3K inhibitor), BYL719 (PI3K-p110α inhibitor), GSK2636771 (PI3K-p110β inhibitor), enzalutamide (AR antagonist), everolimus (mTOR inhibitor of FKBP12), AZD8055 (ATP-competitive mTOR inhibitor), INK128 (mTORC1/2 inhibitor), and XL184 (VEGFR2 inhibitor). All chemicals were stored and their solutions prepared according to the suppliers' recommendations.

Cell lines
The human prostate cancer cell lines LNCaP, 22Rv1, and PC3, as well as the murine Lewis lung carcinoma cell line

Figure 7. **Expression of PSMA in patients allows their stratification in distinct groups that reflect activation of the Akt/mTOR pathway.** (A) Clustering analysis of patient tissue microarray data formed three distinct clusters where elevated PSMA expression correlated with enhanced 4EBP1 phosphorylation in cluster B, whereas decreased PSMA expression was associated with decreased 4EBP1 phosphorylation in cluster C. Cluster A underlines disease and sample heterogeneity, where mixed PSMA staining (sample with PSMA-positive and negative foci) was associated with either lack or low phosphorylation of 4EBP1. The expression of PTEN is displayed but was not considered in the clustering analysis. (B and C) PET/MRI of prostate cancer patients using the PSMA-specific probe ^{68}Ga-HBED-CC, and immunofluorescence microscopy analysis of cancer tissue from patients obtained after prostatectomy. Twelve patients were imaged with PET/MRI, and tissue samples from multiple sites of the biopsy were screened. Representative images are shown, with the corresponding microscopy slides stained for PSMA, pAKT[S473] (Cell Signaling), and Hoechst 33342 (bars, 50 µm). (D and E) Biplot representation suggests that PSMA expression is associated with Akt phosphorylation at residues S473 and T308 and that PSMA immunostaining and PSMA-based PET (SUV values) are both good indicators of Akt's phosphorylation, as these parameters are closer to Akt in the two-dimensional space defined by the primary principal components PC1 and PC2 than other clinical parameters. The open circles show the samples stained per patient and underlie sample variability caused by the heterogeneous nature of the disease. Biplots derived from PCA of patients imaged with PET/MR and their samples underwent histopathological analyses, including immunofluorescence microscopy for phosphorylation of Akt on residues S473 and T308. Gleason, Gleason score; SUVmean, mean standardized uptake value of PSMA tracer. (F) Schematic representation of the overall pathway involving PSMA and induction of tumor-supporting signaling based on our data. Free glutamate released from PSMA after processing of glutamate-containing substrates activates mGluR I receptors found on the plasma membrane of prostate cancer cells. Activation of the glutamatergic system induces downstream calcium signaling and activation of the PI3K cascade, positively regulating tumor growth.

LL2, were obtained from the American Type Culture Collection. All cell lines were regularly tested for mycoplasma contamination and authenticated by DDC Medical through the STR profiling method. The stocks of the human prostate cancer cells lines were grown in a humidified incubator at 37°C, 5% CO_2 and supplemented with RPMI 1640 medium (Gibco) that contained 10% fetal bovine serum (Gemini Bio-products), glutamine ($[Gln]_{fin}$ = 3 mM), 1% Hepes buffer, and 1% penicillin/streptomycin. LL2 cells were grown in DMEM (Gibco) that contained 10% fetal bovine serum and 1% penicillin/streptomycin. To generate cells that lacked PSMA, we used LNCaP cells, which express PSMA, and the Platinum Select retroviral shRNA–mir platform (DU53991) from TransOMIC Technologies, Inc. to knock down the gene PSMA that encodes PSMA (gene ID 2346), following the supplier's guidelines. Selection was done in the presence of puromycin, and confirmation of generation of cells lacking PSMA was achieved with immunoblot analysis, using an anti–human PSMA antibody (YPSMA-1; Abcam). Quantitative real-time PCR was performed by Memorial Sloan Kettering Cancer Center's Integrative Genomics Operation using total RNA extracted with TRIzol (Invitrogen) from cells grown to confluence on Petri dishes, followed by reverse transcription to cDNA using the ProtoScript First Strand cDNA synthesis kit (New England Biolabs), qPCR with the CFX real-time PCR detection system (Bio-Rad), and primer sequences previously reported (Yates et al., 2012). Normalization for PSMA expression was done with LNCaP-Ctrl PSMA expression serving as the calibrator for all samples, and expression of β actin served as an endogenous control. The enzymatically inactive PSMA mutant was generated according to a prior study (Ghosh and Heston, 2003), and the ability of PSMA-expressing cells to process monoglutamated folate, releasing free glutamate in the solution, was determined through Molecular Probes' Amplex Red Glutamic Acid assay following the supplier's protocol (Thermo Fisher Scientific).

Bioinformatics analyses

The GeneChip Human Genome U133A 2.0 array from Affymetrix, Inc. was used to determine gene expression levels in cells expressing or lacking PSMA. Each cell line was analyzed in triplicate, after growth of cells to confluence on Petri dishes, supplemented with complete media. Before total RNA extraction with TRIzol, the cells were washed three times with warm 1× PBS. The preparation of the arrays' samples and subsequent data analysis were done at MSKCC's Integrative Genomics Operation and Bioinformatics Core. To categorize the most differentially affected genes, we determined each gene's function through the NCBI Gene database. The microarray data of the screened PSMA-positive and PSMA-negative human prostate cancer cells have been deposited to the National Center for Biotechnology Information's Gene Expression Omnibus repository (accession no. GSE104419). For the bioinformatics analyses of data from prostate cancer patients, we used a dataset recently reported

(Hieronymus et al., 2014). In brief, from this dataset's initial cohort (n = 168, PMID 25024180), we used the localized cases of primary tumors that have not had any neoadjuvant treatment and matched normal samples of patients that underwent prostatectomy at MSKCC, following institutional review board approval. For gene set enrichment analyses, we used the corresponding gene sets that met the p-value < 0.01, false discovery rate q < 0.2 significance thresholds across the examined cohorts and cell lines. Gene networks were determined and visualized through Cytoscape, based on the intersection of enriched gene sets that meet the significance thresholds in the studied cohorts/cells. PSMA expression was binned as high z >2 expression versus not, and PSMA expression was identified as a prognostic for biochemical recurrence and metastasis even after correcting for the clinical Stephanson nomogram score, which combines other prognostic variables like Gleason score and margins, through multivariate Cox regression. PSMA's association with outcome was examined through a multivariate regression model, which effectively corrects for the nomogram score, which collected all of the clinical and pathological variables, including Gleason grade, into one prognostic variable.

Epifluorescence microscopy for mGluR I and calcium studies in prostate cancer cells

For microscopy studies, the cells were grown on poly(lysine)-coated chamber glass slides at a density of 40,000 cells per chamber. The cells were stained with anti–human PSMA antibody (Dako) and the rabbit polyclonal anti–human mGluR1/5 antibody (Novus Biologicals). Secondary fluorophore-conjugated antibodies were obtained from Abcam, and the nuclear stain Hoechst 33342 was purchased from Invitrogen. The slides were first examined on a Nikon Eclipse Ti-E fluorescence microscope, followed by imaging on the MSKCC's Molecular Cytology Core Leica SP5 laser-scanning confocal microscope (Leica Microsystems, Inc.). To quantify calcium levels, we used the high-throughput Fluo-4 Direct assay from Invitrogen and the SpectraMax M5 plate reader from Molecular Devices. For these studies, cells were seeded at a density of 20,000 cells per well on poly(lysine)-treated black, clear-bottom, 96-well plates (Corning, Inc.), followed by overnight growth. Each well's total volume was set at 100 μl, with cells receiving 10 μl of control (1× PBS) or treatment solution, after dilution of the stock solutions of the various compounds with 1× PBS. Addition of the Fluo-4 reagent, instrument set, and acquisition parameters were performed in accordance to the assay's user handbook, which was provided by the manufacturer.

Identification of PSMA's effect on the activation of signaling pathways

To determine whether PSMA affects the phosphorylation of key kinases, we used the human phosphokinase antibody array from R&D Systems, Inc. (ARY003B) and the PathScan Akt signaling antibody array kit (9700; Cell Signaling, Inc.).

The cells were seeded on poly(lysine)–coated Petri dishes at a density of 1,000,000 cells per dish, followed by 24-h growth at 37°C, 5% CO_2 in complete medium and a 24-h starvation in basal medium. Before the addition of 100 µl control (1× PBS) or experimental treatment, cells were supplemented with fresh media, as mentioned in the figure legends. For compounds whose stock solutions were in DMSO and subsequently diluted in 1× PBS, the corresponding control cell cohort was treated with 1× PBS that contained equimolar concentration of DMSO, with each cohort consisting of three replicates. After incubation with the compounds of interest, the cells were washed three times with chilled 1× PBS, followed by lysis with RIPA buffer (Sigma-Aldrich). The cell lysates were processed according to the recommendations of the arrays' suppliers, and protein concentration was determined using the bicinchoninic acid assay (Pierce Biotechnology). After following the setup and processing steps described in each array's user manual, the arrays were scanned and signal was quantified using the near-infrared fluorescence Odyssey imaging platform (LI-COR Biosciences, Inc.). Changes in phosphorylation were calculated with respect to the corresponding untreated control cells, which were cells of the same background. Evaluation of a protein's global phosphorylation status was determined via changes in its isoelectric point using the NanoPro 1000 system (Protein Simple) and primary rabbit anti–human monoclonal antibodies from Cell Signaling. The cells were prepared and treated similarly to the phosphorylation array studies, followed by lysis with the Bicine/CHAPS buffer (Protein Simple). All reagents and supplies, including sample diluent, ampholyte, standards, and microcapillaries, were purchased from Protein Simple, with the samples prepared according to the guidelines of the instrument's manufacturer, having a protein concentration of 1 µg/µl and same DMSO content as the ampholyte. Detection was achieved through a biotin-conjugated goat anti–rabbit secondary antibody and streptavidin-conjugated horseradish peroxidase using Compass 2.7.1 software for Windows XP to control the instrument and data acquisition and analysis (all from Protein Simple). Human inositol 1,4,5-trisphosphate levels were quantified with the corresponding Cusabio ELISA kit (Cosmo Bio) according to the supplier's guidelines, using cells grown on Petri dishes followed by cell lysis. The SpectraMax M5 microplate reader was used, recording absorbance at 450 nm with the correction wavelength set at 600–630 nm. The activation of Akt by PSMA was determined with the fluorescent substrate of Akt LS456, which exhibits increased fluorescence emission at 700 nm upon phosphorylation by Akt (Shen et al., 2013). LNCaP-Ctrl cells were seeded at 10,000 cells per well on poly(lysine)–coated black, clear-bottom 96-well plates, and after overnight growth in complete media they were administered LS456 ([LS456]$_{fn}$ = 5 µM), as previously reported. After 24 h at 37°C, 5% CO_2, the cells were washed three times with warm 1× PBS, supplemented with 100 µl basal medium that was free of serum, glutamate and folate for 24 h, and then treated with mono-glutamate folate ([Glu-fol]$_{fn}$ = 20 µM) and inhibitors ([inhibitor]$_{fn}$ = 200 nM) for 2 h at 37°C, 5% CO_2, followed by fluorescence emission measurements using the Odyssey platform (LI-COR Biosciences).

Determination of nitric oxidase synthase activity, and quantification of PSA in vitro

The activity of nitric oxidase synthase, which is a downstream target of Akt, was evaluated with the nitric oxide synthase activity kit (Cayman Chemical), following isolation of the cells' extracellular medium. For this, cells were seeded on poly(lysine)–coated Petri dishes at a density of 1,000,000 cells and grown in the presence of complete medium for at 37°C, 5% CO_2 for 48 h. This was followed by aspiration of the media, washing with 1× PBS, and addition of serum-free medium and 2-PMPA. The cells were incubated at 37°C, 5% CO_2, and media were collected at the designated time points, followed by sample processing and analysis in line with the assay-provided protocol. Similarly, the levels of the PSA were determined in the human prostate cancer cell line LNCaP, which expresses the AR and has a functional AR cascade. The cells were cultivated as mentioned above in this section and treated with 2-PMPA for the time indicated in the corresponding figures, followed by media isolation and analysis with the DELFIA Prostatus assay (PerkinElmer).

In vitro and in vivo chemotherapy experiments

Cells were seeded at a density of 20,000 cells per well on poly(lysine)–coated black, clear-bottom, 96-well plates after growth for 24 h in the presence of complete medium at 37°C, 5% CO_2. The medium was then removed, and fresh complete medium was added, which was supplemented with the listed inhibitors. Control wells were treated with 1× PBS or 1× PBS that had equimolar DMSO concentration to correspond to the DMSO concentration of inhibitors whose stock solutions were in DMSO and diluted to the desired compound concentration with 1× PBS. Viability was determined with the Alamar blue assay (Thermo Fisher), after aspirating the treatment medium and addition of 10% Alamar blue–containing fresh medium, and incubation for 3 h at 37°C, 5% CO_2. Inhibition of PSMA with 2-PMPA in LNCaP-Ctrl cells had comparable results with a previous report that used LNCaP cells (Yao and Bacich, 2006). Animal studies were conducted with adult, male, athymic, nude mice obtained from Harlan Laboratories. All animal studies were conducted in accordance to MSKCC's Institutional Animal Care and Use Committee, with procedures approved by MSKCC's Research Animal Resource Center. For the experiment with animals bearing LL2-derived tumors, adult male $PSMA^{-/-}$ C57BL/6J mice were obtained from MSKCC's internal small-animal colony. Xenograft engraftment was achieved by subcutaneous injection of 1,000,000 cells in 100 µl Matrigel on each flank, unless otherwise stated. All compounds were administered i.v. (100 µl), with control cohorts treated with vehicle (1× PBS or 1× PBS with equimolar DMSO

concentration for compounds whose stocks were in DMSO and then diluted to the desired concentration with 1× PBS; DMSO content was less than 2%). Tumor measurements were taken with calipers, and the animals were anesthetized with isoflurane whenever needed. They were euthanized once the tumor reached a diameter of 10 mm, in accordance with institutional policies (maximum tumor volume allowed by Institutional Animal Care and Use Committee was 524 mm^3). Control animals with LNCaP-Ctrl xenografts had established tumors ∼3 wk after xenograft implantation, and the tumors reached the maximum allowable volume within 3 to 4 wk. Drug dosages were based on the compounds' characteristics and to prevent any side effects. For instance, 2-PMPA, which is very hydrophilic and rapidly cleared from the body, was administered at higher concentration than enzalutamide, which is hydrophobic, has 98% protein binding, and has a biological half-life of 9 d. To examine whether PSMA plays a role in early tumor establishment and development, animals were treated with 2-PMPA immediately after xenograft implantation. Imaging studies were conducted at MSKCC's Small Animal Imaging Core facilities using the IVIS Spectrum system (PerkinElmer).

Immunohistochemical examination of xenografts and prostate cancer patient–derived tissue microarray

Human prostate cancer xenografts that were established in adult, male, athymic, nude mice were collected after the animals were euthanized, followed by the excised tumors fixation in 10% neutral-buffered formalin for 48 h. They were then grossed and embedded in paraffin, followed by sectioning to 4 µm onto charged glass slides in the MSKCC Molecular Cytology Core. Immunohistochemical staining and processing was done at HistoWiz, Inc. using human anti–PSMA antibody from Dako and human anti–pAkt1 and pan-Akt antibodies from Cell Signaling. The slides were imaged using the Zeiss MIRAX MIDI slide scanner and Pannoramic Viewer software (3DHistech Ltd.), whereas quantification of immunohistochemistry signal intensity was done with ImageJ after normalization to object count. The tumor tissue microarray was generated from localized prostate cancer specimens obtained from the MSKCC Urology Service, and informed consent was obtained from all subjects. Approval was obtained from the institutional review board and the Human Tissue Utilization Committee before study of human specimens. Immunostaining was done with the human anti–PSMA antibody from Dako and human anti–phospho-4EBP1 and anti–PTEN antibodies from Cell Signaling at the MSK CC Pathology Department.

PET/MRI acquisition

Images were obtained after intravenous injection of ^{68}Ga-HBED-CC constituting an extracellular PSMA ligand synthesized as described previously (Martin et al., 2014). Simultaneous PET/MRI was performed using an integrated whole-body PET/MRI system (Siemens Biograph mMR; Siemens Healthcare), with mpMR-examination that included T2w, DWI, and DCE of the prostate being performed simultaneously during a 15-min PET scan. A workflow chart of this protocol and details for PET-data reconstruction, including the use of the T1w VIBE Dixon for attenuation correction, have been published previously (Souvatzoglou et al., 2013). All reported investigations were conducted in accordance with the Declaration of Helsinki as well as national regulations. Consent to publish photos was obtained from all patients. The retrospective data analysis was approved by the ethics committee of the Technical University of Munich, Germany (permit 5665/13).

Epifluorescence microscopy of histology slides of biopsies from prostate cancer patients imaged with PET/MRI

For further analysis and to obtain additional molecular information, representative tissue sections containing localized prostate cancer were prepared from each radical prostatectomy of the patients undergoing PET/MRI at the Technical University of Munich, Germany. Samples were fixed in 10% neutral-buffered formalin for 48 h, grossed, and embedded in paraffin before sectioning to 4 µm onto charged glass slides. The slides were deparaffinized as follows: twice in xylene for 5 min each, followed by twice in 100% ethanol for 5 min each, followed by twice in 95% ethanol in water for 5 min each and briefly in pure water. Two slides each from nearly all cases were then immediately probed with a solution containing 10% FBS (Gibco) in anti–PSMA antibody (1× 3E6, M3620; Dako) and either anti-pAKT(S473) (4060S, 1:83; Cell Signaling Technologies) or anti-pAKT(T308) (D25E6, 1:83, Cell Signaling Technologies) antibody for 1 h at room temperature. The slides were then washed twice for 5 min each with 1× PBS and then probed with goat anti-mouse secondary antibody-fluorescein conjugate (ab97022, 1:250; Abcam) with chicken anti–rabbit secondary antibody conjugated to Alexa Fluor 647 (A21443, 1:250; Invitrogen) in 1× PBS for 30 min at room temperature. After aspiration of the secondary antibody solution, the slides were then exposed to Hoechst 33342 dye for 1.5 min (H3570, 1:1,000 in 1× PBS; Invitrogen). The slides were then washed twice more with 1× PBS for 5 min each before adding mounting medium (Dako Faramount Aqueous Mounting Medium) and a glass coverslip. The slides were then immediately viewed using a Nikon 80i upright epifluorescence microscope equipped with a Nikon DS-Qi1Mc dark-field CCD camera and excited by a Nikon Intensilight C-HGFI lamp. All images were recorded and processed using Nikon Imaging Software Elements, which was also used for signal quantitation.

Statistics

All data are presented as mean ± SEM unless otherwise stated. P-values were derived from two-tailed Student's *t* tests using the Shapiro–Wilk tests for normally distributed data, the Mann–Whitney *U* tests for nonnormally distributed data, or ANOVA (GraphPad Prism; Graph-

Pad Software, Inc.), with the data meeting appropriate test assumptions. For animal studies determining whether monotherapy to inhibit PSMA's enzymatic activity confers a therapeutic advantage, a priori power analysis identified that the probability is 85% that the study will detect a treatment difference at a two-sided 0.05 significance level, for a sample size of four per independent study group, if the control group experiences tumor growth greater than or equal to 50% from the time treatment commences, where the treatment group experiences tumor stasis or reduction. No animals were excluded, and treatment randomization was applied. Blinding was used, where animals were coded and treatment and tumor measurement did not occur at the same time. No a priori analysis was used to predetermine the animal sample size in combination therapy or nanotherapeutic in vivo studies and evaluation of clinical data. For the tissue microarray and PET-based studies, analyses were performed using the PLS_Toolbox v. 8.0 (Eigenvector Research, Inc.). Specifically for the tissue microarray, the data from 76 patients with localized prostate cancer (PSMA level, PSMA purity, 4EBP1 phosphorylation, and Gleason score) were initially normalized to zero mean and unit variance. A PCA model was generated, with the first two principal components capturing 62.5% of the dataset variance. One patient sample was excluded as an outlier. Based on the principal components, Ward's method was used for clustering the patients, and a dendrogram was created using the Mahalanobis distance. For the patients imaged with PET/MRI using the PSMA-specific PET agent, the samples were separated in two groups based on whether the corresponding histology slides were screened for phosphorylation of Akt at S473 (51 samples from 11 out of 12 patients) or at T308 (72 samples from 12 out of 12 patients), and two PCA models were developed. Additional variables included in the models were the expression levels of PSMA and PSA (low, medium, and high), the Gleason score, and the standardized uptake values from PET (SUV and SUV_{mean}). The biplots, which show the relations of the categorical variables as well as the distribution of the patient samples, are presented, as well as the principal components derived from the analysis.

Online supplemental material

Fig. S1 shows that PSMA expression is up-regulated in cancer. Fig. S2 shows that enzymatically active PSMA is required to activate p110b-dependent downstream signaling. Fig. S3 shows that PSMA processes glutamated folates in prostate cancer and that the released glutamate activates mGluR I. Fig. S4 shows that PSMA activates the PI3K–Akt axis in vitro and in prostate cancer patients. Fig. S5 shows in vivo evaluation of the inhibition of PSMA as a potential therapy in prostate cancer. Table S1 shows expression of PSMA associates with biochemical recurrence in prostate cancer patients. Table S2 shows expression of PSMA associates with metastasis in prostate cancer patients.

REFERENCES

Carver, B.S., C. Chapinski, J. Wongvipat, H. Hieronymus, Y. Chen, S. Chandarlapaty, V.K. Arora, C. Le, J. Koutcher, H. Scher, et al. 2011. Reciprocal feedback regulation of PI3K and androgen receptor signaling in PTEN-deficient prostate cancer. Cancer Cell. 19:575–586. https://doi.org/10.1016/j.ccr.2011.04.008

Chang, S.S., D.S. O'Keefe, D.J. Bacich, V.E. Reuter, W.D. Heston, and P.B. Gaudin. 1999. Prostate-specific membrane antigen is produced in tumor-associated neovasculature. Clin. Cancer Res. 5:2674–2681.

Cizmecioglu, O., J. Ni, S. Xie, J.J. Zhao, and T.M. Roberts. 2016. Rac1-mediated membrane raft localization of PI3K/p110β is required for its activation by GPCRs or PTEN loss. eLife. 5:e17635. https://doi.org/10.7554/eLife.17635

Cohen-Solal, K.A., R.K. Boregowda, and A. Lasfar. 2015. RUNX2 and the PI3K/AKT axis reciprocal activation as a driving force for tumor progression. Mol. Cancer. 14:137. https://doi.org/10.1186/s12943-015-0404-3

Colombatti, M., S. Grasso, A. Porzia, G. Fracasso, M.T. Scupoli, S. Cingarlini, O. Poffe, H.Y. Naim, M. Heine, G. Tridente, et al. 2009. The prostate specific membrane antigen regulates the expression of IL-6 and CCL5 in prostate tumour cells by activating the MAPK pathways. PLoS One. 4:e4608. https://doi.org/10.1371/journal.pone.0004608

Dienstmann, R., J. Rodon, V. Serra, and J. Tabernero. 2014. Picking the point of inhibition: a comparative review of PI3K/AKT/mTOR pathway inhibitors. Mol. Cancer Ther. 13:1021–1031. https://doi.org/10.1158/1535-7163.MCT-13-0639

Eder, M., M. Schäfer, U. Bauder-Wüst, W.E. Hull, C. Wängler, W. Mier, U. Haberkorn, and M. Eisenhut. 2012. 68Ga-complex lipophilicity and the targeting property of a urea-based PSMA inhibitor for PET imaging. *Bioconjug. Chem.* 23:688–697. https://doi.org/10.1021/bc200279b

El Sheikh, S.S., H.M. Romanska, P. Abel, J. Domin, and N. Lalani. 2008. Predictive value of PTEN and AR coexpression of sustained responsiveness to hormonal therapy in prostate cancer--a pilot study. *Neoplasia.* 10:949–953. https://doi.org/10.1593/neo.08582

Evans, M.J., P.M. Smith-Jones, J. Wongvipat, V. Navarro, S. Kim, N.H. Bander, S.M. Larson, and C.L. Sawyers. 2011. Noninvasive measurement of androgen receptor signaling with a positron-emitting radiopharmaceutical that targets prostate-specific membrane antigen. *Proc. Natl. Acad. Sci. USA.* 108:9578–9582. https://doi.org/10.1073/pnas.1106383108

Ferté, C., F. André, and J.C. Soria. 2010. Molecular circuits of solid tumors: prognostic and predictive tools for bedside use. *Nat. Rev. Clin. Oncol.* 7:367–380. https://doi.org/10.1038/nrclinonc.2010.84

Ghosh, A., and W.D. Heston. 2003. Effect of carbohydrate moieties on the folate hydrolysis activity of the prostate specific membrane antigen. *Prostate.* 57:140–151. https://doi.org/10.1002/pros.10289

Gonzalez-Guerrico, A.M., J. Meshki, L. Xiao, F. Benavides, C.J. Conti, and M.G. Kazanietz. 2005. Molecular mechanisms of protein kinase C–induced apoptosis in prostate cancer cells. *J. Biochem. Mol. Biol.* 38:639–645.

Hieronymus, H., N. Schultz, A. Gopalan, B.S. Carver, M.T. Chang, Y. Xiao, A. Heguy, K. Huberman, M. Bernstein, M. Assel, et al. 2014. Copy number alteration burden predicts prostate cancer relapse. *Proc. Natl. Acad. Sci. USA.* 111:11139–11144. https://doi.org/10.1073/pnas.1411446111

Hrkach, J., D. Von Hoff, M. Mukkaram Ali, E. Andrianova, J. Auer, T. Campbell, D. De Witt, M. Figa, M. Figueiredo, A. Horhota, et al. 2012. Preclinical development and clinical translation of a PSMA-targeted docetaxel nanoparticle with a differentiated pharmacological profile. *Sci. Transl. Med.* 4:128ra39. https://doi.org/10.1126/scitranslmed.3003651

Huang, W., P.J. Zhu, S. Zhang, H. Zhou, L. Stoica, M. Galiano, K. Krnjević, G. Roman, and M. Costa-Mattioli. 2013. mTORC2 controls actin polymerization required for consolidation of long-term memory. *Nat. Neurosci.* 16:441–448. https://doi.org/10.1038/nn.3351

Jia, S., Z. Liu, S. Zhang, P. Liu, L. Zhang, S.H. Lee, J. Zhang, S. Signoretti, M. Loda, T.M. Roberts, and J.J. Zhao. 2008. Essential roles of PI(3)K-p110beta in cell growth, metabolism and tumorigenesis. *Nature.* 454:776–779.

Jiang, X., S. Chen, J.M. Asara, and S.P. Balk. 2010. Phosphoinositide 3-kinase pathway activation in phosphate and tensin homolog (PTEN)–deficient prostate cancer cells is independent of receptor tyrosine kinases and mediated by the p110beta and p110delta catalytic subunits. *J. Biol. Chem.* 285:14980–14989. https://doi.org/10.1074/jbc.M109.085696

Josselyn, S.A., and P.W. Frankland. 2013. mTORC2: actin on your memory. *Nat. Neurosci.* 16:379–380. https://doi.org/10.1038/nn.3362

Klusák, V., C. Barinka, A. Plechanovová, P. Mlcochová, J. Konvalinka, L. Rulísek, and J. Lubkowski. 2009. Reaction mechanism of glutamate carboxypeptidase II revealed by mutagenesis, X-ray crystallography, and computational methods. *Biochemistry.* 48:4126–4138. https://doi.org/10.1021/bi900220s

Kratochwil, C., F. Bruchertseifer, F.L. Giesel, M. Weis, F.A. Verburg, F. Mottaghy, K. Kopka, C. Apostolidis, U. Haberkorn, and A. Morgenstern. 2016. 225Ac-PSMA-617 for PSMA-Targeted alpha-Radiation Therapy of Metastatic Castration-Resistant Prostate Cancer. *J. Nucl. Med.* 57:1941–1944. https://doi.org/10.2967/jnumed.116.178673

Martin, R., S. Jüttler, M. Müller, and H.J. Wester. 2014. Cationic eluate pretreatment for automated synthesis of [68Ga]CPCR4.2. *Nucl. Med. Biol.* 41:84–89. https://doi.org/10.1016/j.nucmedbio.2013.09.002

Maurer, T., J.E. Gschwend, I. Rauscher, M. Souvatzoglou, B. Haller, G. Weirich, H.J. Wester, M. Heck, H. Kubler, A.J. Beer, et al. 2016. Diagnostic Efficacy of 68Gallium-PSMA Positron Emission Tomography Compared to Conventional Imaging in Lymph Node Staging of 130 Consecutive Patients with Intermediate to High Risk Prostate Cancer. *J. Urol.* 195:1436–1443. https://doi.org/10.1016/j.juro.2015.12.025

Mitsiades, N. 2013. A road map to comprehensive androgen receptor axis targeting for castration-resistant prostate cancer. *Cancer Res.* 73:4599–4605. https://doi.org/10.1158/0008-5472.CAN-12-4414

Nesbitt, H., G. Browne, K.M. O'Donovan, N.M. Byrne, J. Worthington, S.R. McKeown, and D.J. McKenna. 2016. Nitric Oxide Up-Regulates RUNX2 in LNCaP Prostate Tumours: Implications for Tumour Growth In Vitro and In Vivo. *J. Cell. Physiol.* 231:473–482. https://doi.org/10.1002/jcp.25093

Pandit-Taskar, N., J.A. O'Donoghue, J.C. Durack, S.K. Lyashchenko, S.M. Cheal, V. Beylergil, R.A. Lefkowitz, J.A. Carrasquillo, D.F. Martinez, A.M. Fung, et al. 2015. A Phase I/II Study for Analytic Validation of 89Zr-J591 ImmunoPET as a Molecular Imaging Agent for Metastatic Prostate Cancer. *Clin. Cancer Res.* 21:5277–5285. https://doi.org/10.1158/1078-0432.CCR-15-0552

Perner, S., M.V. Cronauer, A.J. Schrader, H. Klocker, Z. Culig, and A. Baniahmad. 2015. Adaptive responses of androgen receptor signaling in castration-resistant prostate cancer. *Oncotarget.* 6:35542–35555. https://doi.org/10.18632/oncotarget.4689

Price, A.J., R.C. Travis, P.N. Appleby, D. Albanes, A. Barricarte Gurrea, T. Bjørge, H.B. Bueno-de-Mesquita, C. Chen, J. Donovan, R. Gislefoss, et al. Endogenous Hormones, Nutritional Biomarkers, and Prostate Cancer Collaborative Group. 2016. Circulating Folate and Vitamin B12 and Risk of Prostate Cancer: A Collaborative Analysis of Individual Participant Data from Six Cohorts Including 6875 Cases and 8104 Controls. *Eur. Urol.* 70:941–951. https://doi.org/10.1016/j.eururo.2016.03.029

Rahbar, K., H. Ahmadzadehfar, C. Kratochwil, U. Haberkorn, M. Schafers, M. Essler, R.P. Baum, H.R. Kulkarni, M. Schmidt, A. Drzezga, et al. 2017. German Multicenter Study Investigating 177Lu-PSMA-617 Radioligand Therapy in Advanced Prostate Cancer Patients. *J. Nucl. Med.* 58:85–90. https://doi.org/10.2967/jnumed.116.183194

Rahn, K.A., B.S. Slusher, and A.I. Kaplin. 2012a. Glutamate in CNS neurodegeneration and cognition and its regulation by GCPII inhibition. *Curr. Med. Chem.* 19:1335–1345. https://doi.org/10.2174/092986712799462649

Rahn, K.A., C.C. Watkins, J. Alt, R. Rais, M. Stathis, I. Grishkan, C.M. Crainiceau, M.G. Pomper, C. Rojas, M.V. Pletnikov, et al. 2012b. Inhibition of glutamate carboxypeptidase II (GCPII) activity as a treatment for cognitive impairment in multiple sclerosis. *Proc. Natl. Acad. Sci. USA.* 109:20101–20106. https://doi.org/10.1073/pnas.1209934109

Rajasekaran, A.K., G. Anilkumar, and J.J. Christiansen. 2005. Is prostate-specific membrane antigen a multifunctional protein? *Am. J. Physiol. Cell Physiol.* 288:C975–C981. https://doi.org/10.1152/ajpcell.00506.2004

Reid, A.H., G. Attard, L. Ambroisine, G. Fisher, G. Kovacs, D. Brewer, J. Clark, P. Flohr, S. Edwards, D.M. Berney, et al. Transatlantic Prostate Group. 2010. Molecular characterisation of ERG, ETV1 and PTEN gene loci identifies patients at low and high risk of death from prostate cancer. *Br. J. Cancer.* 102:678–684. https://doi.org/10.1038/sj.bjc.6605554

Ristau, B.T., D.S. O'Keefe, and D.J. Bacich. 2014. The prostate-specific membrane antigen: lessons and current clinical implications from 20 years of research. *Urol. Oncol.* 32:272–279. https://doi.org/10.1016/j.urolonc.2013.09.003

Schwartz, S., J. Wongvipat, C.B. Trigwell, U. Hancox, B.S. Carver, V. Rodrik-Outmezguine, M. Will, P. Yellen, E. de Stanchina, J. Baselga, et al. 2015. Feedback suppression of PI3Kα signaling in PTEN-mutated tumors is relieved by selective inhibition of PI3Kβ. *Cancer Cell.* 27:109–122. https://doi.org/10.1016/j.ccell.2014.11.008

Shankar, E., K. Song, S.L. Corum, K.L. Bane, H. Wang, H.Y. Kao, and D. Danielpour. 2016. A Signaling Network Controlling Androgenic

Repression of c-Fos Protein in Prostate Adenocarcinoma Cells. *J. Biol. Chem*. 291:5512–5526. https://doi.org/10.1074/jbc.M115.694877

Shen, D., M. Bai, R. Tang, B. Xu, X. Ju, R.G. Pestell, and S. Achilefu. 2013. Dual fluorescent molecular substrates selectively report the activation, sustainability and reversibility of cellular PKB/Akt activity. *Sci. Rep.* 3:1697. https://doi.org/10.1038/srep01697

Souvatzoglou, M., M. Eiber, A. Martinez-Moeller, S. Fürst, K. Holzapfel, T. Maurer, S. Ziegler, S. Nekolla, M. Schwaiger, and A.J. Beer. 2013. PET/MR in prostate cancer: technical aspects and potential diagnostic value. *Eur. J. Nucl. Med. Mol. Imaging.* 40(S1, Suppl 1):S79–S88. https://doi.org/10.1007/s00259-013-2445-4

Sweat, S.D., A. Pacelli, G.P. Murphy, and D.G. Bostwick. 1998. Prostate-specific membrane antigen expression is greatest in prostate adenocarcinoma and lymph node metastases. *Urology.* 52:637–640. https://doi.org/10.1016/S0090-4295(98)00278-7

Tanaka, Y., M.V. Gavrielides, Y. Mitsuuchi, T. Fujii, and M.G. Kazanietz. 2003. Protein kinase C promotes apoptosis in LNCaP prostate cancer cells through activation of p38 MAPK and inhibition of the Akt survival pathway. *J. Biol. Chem*. 278:33753–33762. https://doi.org/10.1074/jbc.M303313200

Taylor, B.S., N. Schultz, H. Hieronymus, A. Gopalan, Y. Xiao, B.S. Carver, V.K. Arora, P. Kaushik, E. Cerami, B. Reva, et al. 2010. Integrative genomic profiling of human prostate cancer. *Cancer Cell*. 18:11–22. https://doi.org/10.1016/j.ccr.2010.05.026

Xiao, L., A. Gonzalez-Guerrico, and M.G. Kazanietz. 2009. PKC-mediated secretion of death factors in LNCaP prostate cancer cells is regulated by androgens. *Mol. Carcinog.* 48:187–195. https://doi.org/10.1002/mc.20476

Yao, V., and D.J. Bacich. 2006. Prostate specific membrane antigen (PSMA) expression gives prostate cancer cells a growth advantage in a physiologically relevant folate environment in vitro. *Prostate.* 66:867–875. https://doi.org/10.1002/pros.20361

Yao, V., A. Parwani, C. Maier, W.D. Heston, and D.J. Bacich. 2008. Moderate expression of prostate-specific membrane antigen, a tissue differentiation antigen and folate hydrolase, facilitates prostate carcinogenesis. *Cancer Res.* 68:9070–9077. https://doi.org/10.1158/0008-5472.CAN-08-2328

Yates, D.R., M. Rouprêt, S.J. Drouin, E. Comperat, S. Ricci, R. Lacave, P. Sèbe, G. Cancel-Tassin, M.O. Bitker, and O. Cussenot. 2012. Quantitative RT-PCR analysis of PSA and prostate-specific membrane antigen mRNA to detect circulating tumor cells improves recurrence-free survival nomogram prediction after radical prostatectomy. *Prostate.* 72:1382–1388. https://doi.org/10.1002/pros.22488

Yu, L.J., B.A. Wall, J. Wangari-Talbot, and S. Chen. 2017. Metabotropic glutamate receptors in cancer. *Neuropharmacology.* 115:193–202. https://doi.org/10.1016/j.neuropharm.2016.02.011

Yuan, X., C. Cai, S. Chen, S. Chen, Z. Yu, and S.P. Balk. 2014. Androgen receptor functions in castration-resistant prostate cancer and mechanisms of resistance to new agents targeting the androgen axis. *Oncogene.* 33:2815–2825. https://doi.org/10.1038/onc.2013.235

Zhou, J., J.H. Neale, M.G. Pomper, and A.P. Kozikowski. 2005. NAAG peptidase inhibitors and their potential for diagnosis and therapy. *Nat. Rev. Drug Discov.* 4:1015–1026. https://doi.org/10.1038/nrd1903